Chapter 6

Tracking

This section describes the tracking detectors, their required performance and design. The forward spectrometer and the midrapidity spectrometer are dealt with in separate sections. The design criteria are somewhat different for the two spectrometer arms due to the different momentum ranges to be covered. Both arms will have TPC's as tracking detectors. At the present time a detailed design for the tracking detector has not been developed, but as described in Section 6.3, a prototype TPC has been built at Strasbourg and is undergoing tests. These tests as well as simulations will form the basis for a final design. The requirements in terms of size, number of pad rows for the TPC's and number of wire planes for the drift chambers in the Forward Arm are well understood.

6.1 Forward Spectrometer

The tracking of particles in the spectrometer involves several overlapping considerations. The first is the optics and layout of the spectrometers, which determines acceptance, multiplicities of particles, etc., in the different detectors. The second is how to determine the momenta of particles reconstructed through the tracking detectors, and the third the design of these detector components. This report deals mainly with the first two issues, and only discusses the conceptual design of the forward spectrometer tracking detectors.

6.1.1 General tracking considerations

The design of the spectrometer comes from some fairly simple tracking criteria. That the actual choice is workable is also confirmed through extensive simulations.

As has been described in the overview the forward spectrometer will be operating in two different modes.

- High-momentum mode. The forward-going particles are swept by the dipoles D1 and D2 towards the back end of the spectrometer where they are tracked in the chambers T2, T3, T4 and T5. Their momenta are determined by these measurements and the knowledge that they passed though the dipoles D3 and D4. The particle identification (PID) is done after D4 and T5. The particles are traced back to T2, and their trajectories projected back through D2 and D1 to confirm that they arose from the interaction point, and not from secondary scattering on polefaces, etc. The tracks must be found in T2, but not necessarily in T1.

- Low-momentum mode. The particles are tracked by T1 and T2 and their momenta determined by the dipole D2. The PID is done right after T2. The particles are projected back through D1 towards the

  interaction point to ensure their validity. This mode is used both at forward angles and at angles up to 30°.

These two modes of operation set the requirements on the tracking detectors.

Position and angular resolution

In the spectrometer system it is necessary to follow segments of a track from measurements in one tracking detector to the matching track segments in another element. This involves typical distances of 4 m. Several factors contribute to how well this can be done. First are the physical processes, such multiple scattering, which affect the tracks. For high momentum tracks this effect is usually small and can thus be dealt with. The variance due to multiple scattering for pions and protons passing through 4 meters of air has been evaluated using the following expression:

$$y^{rms}_{plane} = \frac{1}{\sqrt{3}}\theta_0 \ ,$$

where

$$\theta_0 = \frac{13.6}{\beta p}\sqrt{X/X_0}\ (1 + 0.038\ \ln(X/X_0)) \ ,$$

p is the momentum in GeV/c, βc is the velocity, X/X_0 is the thickness of the scattering medium in radiation lengths and y^{rms}_{plane} is the variance in a given plane at distance X. This relation is plotted in Fig. 6.1. It is observed that for particles with momenta above 2 GeV/c this contribution is less than 1 mm.

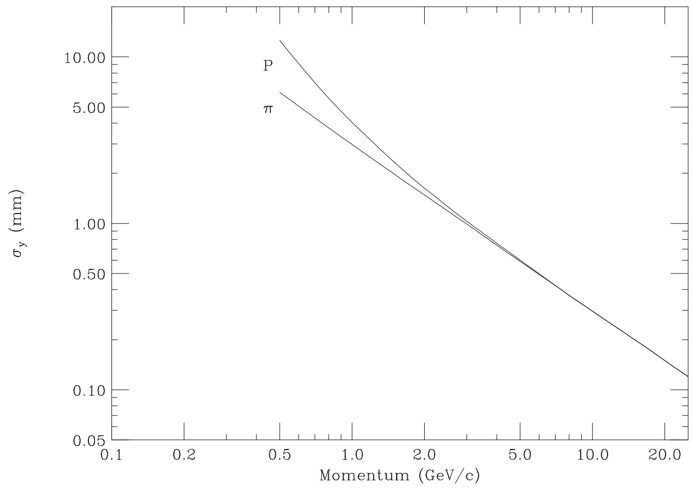

Figure 6.1: Variance due to multiple scattering over 4 meters of air.

A more important factor in the ability to project tracks is the accuracy of position measurements in the tracking detectors. Assume for simplicity that tracks are measured at the entrance and exit of each tracking detector with a resolution σ_D. Then the track can be traced back a distance X with an accuracy given by

$$\sigma_y \approx 2\sigma_D X/L_{det} \ ,$$

where L_{det} is the length of the detector volume. As an example, a detector with length $L_{det} = 80$ cm, a distance $X = 4$ m and the condition that $\sigma_y \leq 2$mm requires the resolution $\sigma_D \leq 285 \ \ \mu$m . The condition is reasonable for matching the tracks and the required position resolution is not difficult to achieve.

The momentum resolution of the spectrometer is given to first order by

$$\frac{\delta p}{p} = \frac{\delta\theta}{\theta} = \frac{2\sigma_D p}{0.30 \, Bdl \, L_{det}} \ ,$$

where Bdl is in T-m integrated through D3 and D4. For the momentum setting which covers 7.5-15 GeV/c and $Bdl = 2.4$ Tm we calculate $\delta p/p = p \times 0.09\%$, where p is in GeV/c.

To confirm that the above-mentioned criteria are indeed fulfilled a GEANT simulation with tracking was performed. Specifically, 10 GeV/c pions were emitted from the interaction point, traced through the spectrometer system, and their hits recorded at the entrance and exit of all detector elements. The tracking algorithm used this information with an assumed position resolution of 200 μm to match track segments, reconstruct the momentum and follow the tracks using the procedure outlined above for the high-momentum setting. The extracted $\delta p/p$ distribution is shown in the left-most frame of Fig. 6.2.

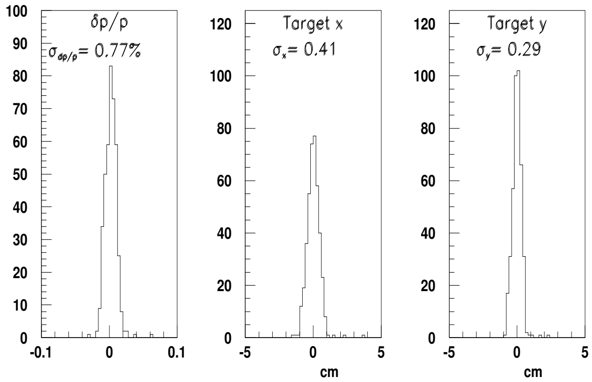

Figure 6.2: Reconstructed momentum resolution, target position distributions for 10 GeV/c pions with an assumed position resolution of 200 μm .

.

In the other two frames are shown the projected target positions. Note that even over the lever arm of 8 m from T2 to the interaction point the distribution is determined to better than 5 mm. In Table 6.1 below is shown the variance as a function of the assumed detector resolution.

σ_D μm	σ_p/p %	σ_x mm	σ_y mm
100	0.39	2.2	1.9
200	0.77	4.1	2.9
250	1.00	5.1	3.6
300	1.15	6.5	4.6

Table 6.1: Resolution of momentum and of determined target position as a function of the intrinsic detector resolution for 10 GeV/c π^-.

Particle Multiplicities

Of great importance to the detector design are the particle multiplicities and particle densities with which each detector element must contend. These quantities have been evaluated using GEANT simulations with 400 central Au+Au events from VENUS as input, and the results are summarized in Tables 6.2 , 6.3 and 6.4. The estimates do of course depend critically on the angular and magnetic field settings. Here we consider three cases which are important and the most difficult to deal with.

- Spectrometer at 2.1° setup for intermediate momentum acceptance, i.e., $p = 7.5 - 15$ GeV/c.
- Spectrometer at 2.1° setup for high momentum acceptance, i.e., $p = 15 - 30$ GeV/c.
- Spectrometer at 2.1° for low momentum setting, i.e., $p = 2 - 5$ GeV/c. For this setting D2 is rotated 5° relative to D1 whereas in the normal mode of operation D2 is only rotated 1.8°.

Only particles which were emitted toward the first dipole D1 were tracked. A discussion of background from other sources is presented later. In addition to the primary particles

Detector	N_{prim}	N_{sec}	N_{total}	particles/cm^2
T2	4.1	3.5	7.6	0.02
T3	2.7	4.4	7.1	0.007
T4	1.5	0.8	2.4	0.002
T5	1.0	0.5	1.6	0.001

Table 6.2: Expected charged particle multiplicities for the 7.5-15 GeV/c setting at 2.1°.

emitted from the interaction, secondaries are generated primarily from the magnet yokes and field clamps, and to a lesser extent from the detectors.

Detector	N_{prim}	N_{sec}	N_{total}	particles/cm^2
T2	2.2	2.5	4.7	0.01
T3	1.2	4.6	5.9	0.006
T4	0.6	1.0	1.6	0.001
T5	0.3	0.5	0.8	0.0004

Table 6.3: Expected charged particle multiplicities for the 15-30 GeV/c setting at 2.1°.

The expected multiplicities are presented in the tables above. It can be observed that near the end of the spectrometer, i.e. in T4 and T5, the expected multiplicities are quite low, with the typical number of charged particles being 0.5–2. This sets only modest requirements for the tracking and PID detectors. On the other hand the charged particle multiplicities in T2 and T3 are higher and reach values of up to 8. The fairly high background rate in T3 is due to particles coming though the spectrometer which produce secondary emissions in the beamline magnet DX. Even for T1 the particle densities are acceptable for all settings.

Detector	N_{prim}	N_{sec}	N_{total}	particles/cm^2
T1	6.6	10.0	16.5	0.04
T2	2.4	1.4	3.8	0.01

Table 6.4: Expected charged particle multiplicities for the 2-5 GeV/c setting at 2.1°.

Detector	Primary	Background No Shield	Background With Shield
T2	4.3	11.8	5.3
H1	3.8	10.2	5.9

Table 6.5: Effect of shielding on rates per central Au+Au event in T1, T2 and H1 of the forward arm.

Shielding of Detectors

The very large expected multiplicity for central Au+Au collisions will make the background conditions difficult. For the forward angle measurements backgrounds generated from forward-going particles interacting in the magnet yoke, beam pipe, pump cluster and DX beam line magnet could contribute significantly to the observed multiplicity rates in the tracking and PID detectors. It would thus appear that some shielding of the detectors is needed. However, introduction of shielding for an experimental apparatus is often problematic, since it adds material from which additional secondary particles might be generated.

The T2 tracking detector plays an important role in the overall tracking of the forward spectrometer, and was thus taken as the focus for background considerations. The other tracking detectors (T3, T4, T5) being farther away from the interaction diamond have less background and can be more easily shielded. The proximity of T2 to the beam pipe makes it an obvious candidate for shielding. The layout of the shielding considered is depicted in Fig. 6.3. The expected background with this configuration has been estimated from several Monte Carlo runs. The shielding was envisioned to be made primarily of Pb, $\approx$ 50cm in height with a trapezoidal shape and attached to the D2 magnet and platform. (Heavymet was rejected due to cost.)

Since Monte Carlo calculations are very time consuming, the phase space considered for reaction products was confined to those emitted with polar angles less than 8°; i.e. all particles emerging towards the spectrometer and down the beamline. The results are summarized in Table 6.5 for rates of charged particles per central event.

Of the 5.3 background particles in T2, with shielding included, we know that approximately 3 come from interactions inside the magnets. Thus the increase of the charged

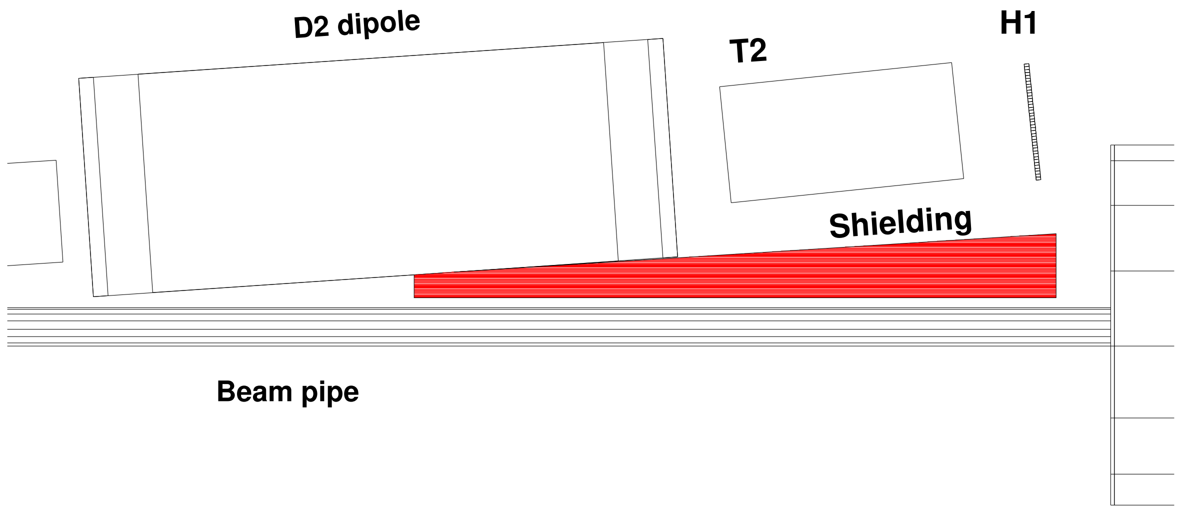

Figure 6.3: Top view of shielding for T2

particle background due to interactions in the beam pipe and shielding is approximately 2. This can easily be handled by the proposed tracking detectors. The simulations do not have a detailed description of the detector modules, and hence some additional background might be expected. However, the excellent pattern recognition capabilities of the T2 TPC will enable us to easily separate valid trucks from background tracks.

The H1 segmentation of 40 results in an average occupancy of approximately 20% for central Au+Au events at 2.1°. This can be tolerated since the measurements are inclusive. In addition it should be remembered that H1 is not the primary PID detector for the high momentum measurements but will be used to confirm the measurements in the H2 and RICH detectors.

6.1.2 Tracking Detectors

The tracking detectors T1-T5 have yet to be designed in detail, but the required capabilities are clear from the design criteria and the multiplicity considerations given above. The detectors T1, T2 and perhaps also T3 will be TPCs with good pattern recognition capabilities and intrinsic position resolution of $\approx$350 μm.

To avoid duplication of effort in detector design it was decided to use the same modular readout chambers for T1 and T2 TPC as will be used in the TPC's for the mid-rapidity spectrometer. This sets the active width for T1 and T2 to be 25 cm using a 4 mm pad spacing. The number of pad rows have been determined from simulations using the track reconstruction program SONATA (See Appendix B). The quality of local track reconstruction was judged from visual inspection of the Monte Carlo events and

Tracking Detector	width (cm)	height (cm)	length (cm)	# planes	# channels/wires	
T1	25	15	75	16	1024	chan.
T2	25	20	75	10	640	
T3	35	30	75	24	430	wires
T4	40	35	75	22	420	
T5	45	40	75	18	350	

Table 6.6: Detector characteristics for the forward arm components.

the reconstructed tracks.

The dimensions of the detectors and an approximate channel count are given in Table 6.6. The position and angular resolution resulting from sampling the track parameters on 10 rows satisfy the requirement $\delta x <$200 μm and $\delta\theta < 0.5$ mrad.

The tracking detectors T5, T4 and perhaps also T3, are envisioned to be drift chambers, each set up in 3 submodules placed at -35, 0 and +35 cm in each detector, allowing for both pattern recognition and subsequent track segment determination to a position resolution of $\approx$ 200-250 μm over the detector length of 80 cm. See Fig. 6.4 for an illustration of the layout with 3 submodules . Each submodule will consist of planes with approximately 1-cm wire spacing in a staggered geometry xx'yy'uv[xx']. (The last xx' planes may be omitted in the T5 detector.) The dimensions of the detectors and approximate channel counts are given in Table 6.6 for all five detectors T1 through T5.

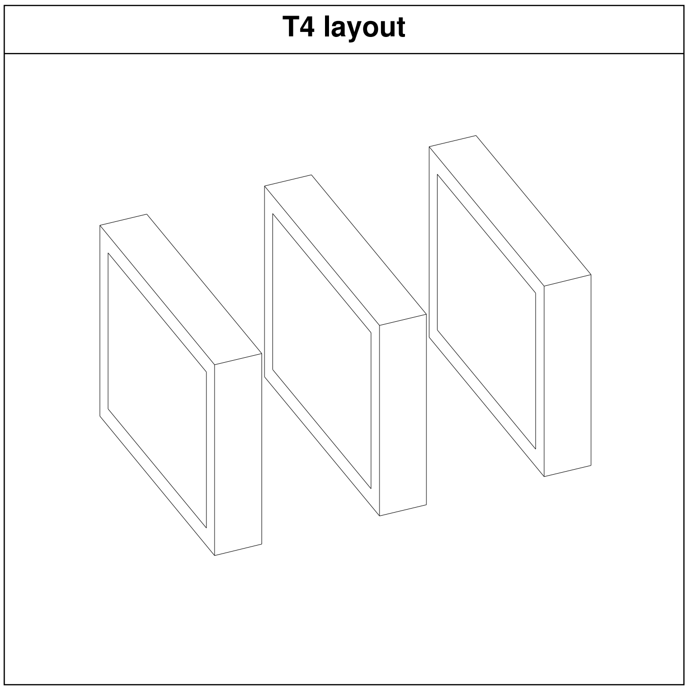

Figure 6.4: Schematic layout of T4 with 3 separate submodules of drift chambers separated by 35 cm. Each package will consist of 6 to 8 planes of drift chambers.

6.2 Midrapidity Spectrometer

The mid-rapidity spectrometer of BRAHMS (see Section 3.2) is designed to determine the momenta of individual particles by following their tracks through a magnetic field and identifying them by time-of-flight, Čerenkov and momentum measurements. The basic requirements for this spectrometer are:

- Locate all charged particle tracks (π,K,p) which originate from the interaction diamond.
- Measure momenta.
- Contribute to the particle identification (PID) completed in association with the scintillator time-of-flight wall (TOFW) and the gas Čerenkov counter (GASC).

This detector ensemble will be in an environment of high track density. The expected multiplicities and particle densities have been estimated by using the VENUS 4.02 model for central Au+Au collisions at $\sqrt{s} = 200$ GeV. The nominal setting of 34° (which in fact covers 30° to 38°) is the most difficult case to deal with, and has driven the design of the midrapidity spectrometer. Due to the low momentum of the particles, it is an advantage to have the detectors and magnet situated as close as possible to the intersection point; on the other hand, an important design criterion is that the particle density in the front TPC be less than 0.3 particle/cm^2. To achieve this goal the midrapidity system has been placed with magnet D5 at 190 cm from the nominal intersection point and TPC1 at 90 cm. At the most forward angles the distributions are not uniform, as depicted in Figure 6.5, which shows the particle densities in the front TPC and the TOF wall at the nominal 34° setting for central Au+Au collisions. In the mid-rapidity spectrometer angular domain, the multiplicities including secondary charged particles range from 30 to 120 whereas the particle densities range from < 0.01 to 0.20 particle/cm^2 (see Table 6.7.) An overview of the particle multiplicities is given in Figure 6.6. The hit multiplicity in TPC2 is less than in TPC1 because of the smaller solid angle and because of the sweeping of particles due to the magnetic field; in Table 6.7 the field in D5 is taken as 4 kG.

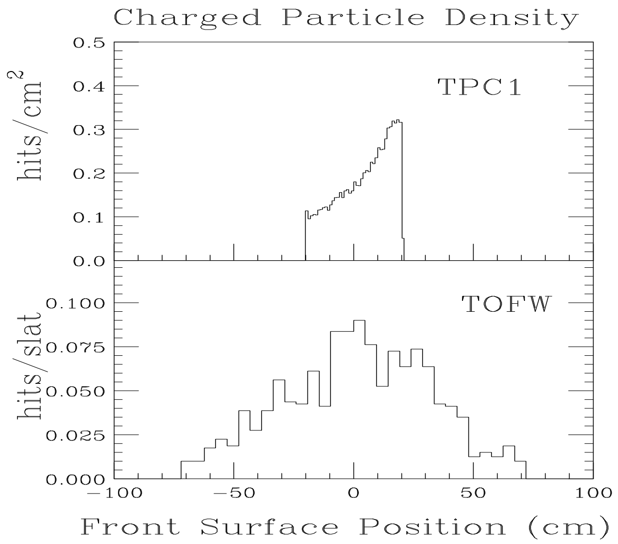

Figure 6.5: Charged particle densities in the midrapidity front TPC and TOF wall for the nominal 34° setting.

To improve the tracking capabilities by reducing both the multiple scattering and the energy loss for low momentum particles it is planned to install a helium bag inside the gap of D5.

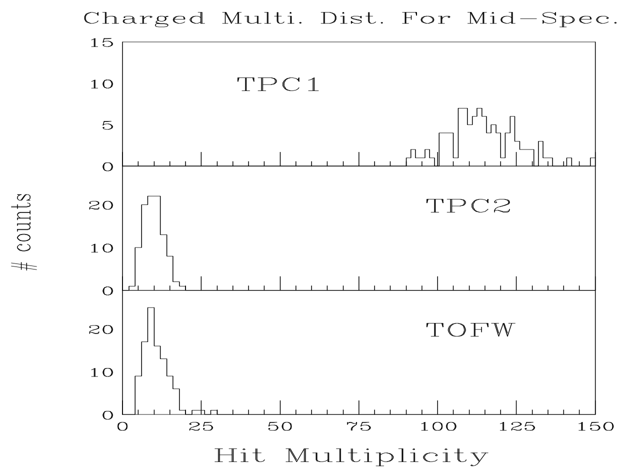

Figure 6.6: Hit multiplicities in the midrapidity TPC's and TOF wall for the nominal 34° setting.

	primary	secondary	total	particles/cm^2
34°				
TPC1	101	12	113	0.19
TPC2	7	2	9	0.01
TOFW	7	5	12	
90°				
TPC1	30	5	35	0.05
TPC2	2	1	3	0.003
TOFW	2	1.4	3.4	

Table 6.7: Average charged particle multiplicities in the midrapidity spectrometer.

6.3 Time Projection Chambers

6.3.1 Design of the Midrapidity TPC's

In order to obtain the best momentum resolution, even at low values of the momentum, one needs to minimize the amount of material in front of and in the volume of the tracking detectors. For this reason the tracking is achieved by two time projection chambers (TPC's) with the particle identification performed in separate detectors (TOFW and GASC). Precise momentum determinations are achieved by two TPC's providing three-dimensional position measurements of each particle track. These detectors, TPC1

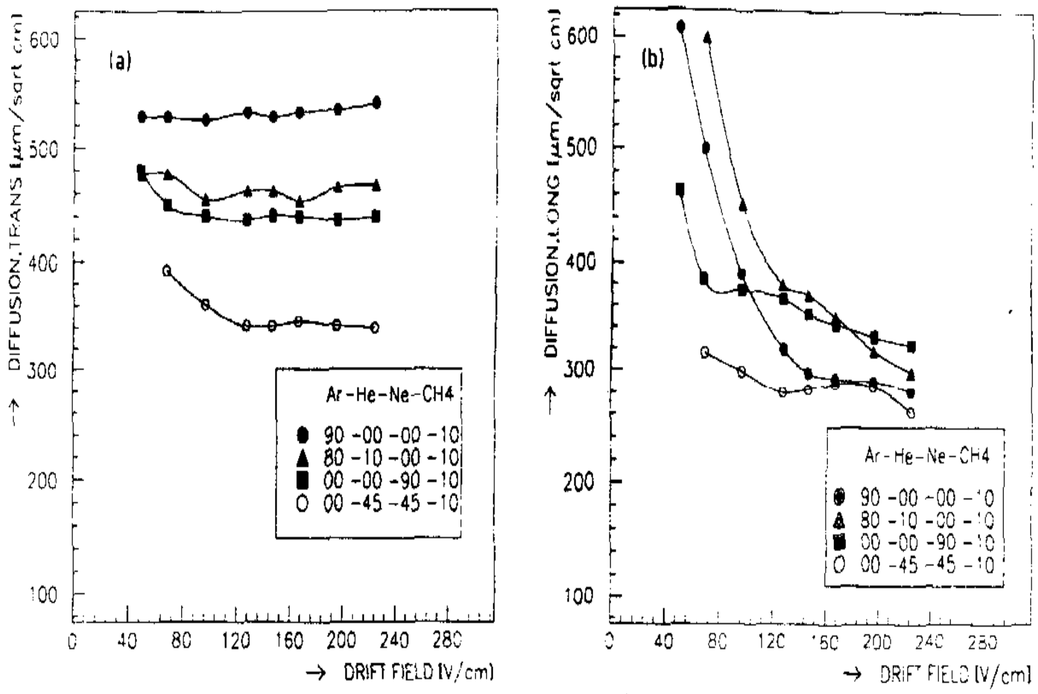

Figure 6.7: Longitudinal and transverse diffusion constants for various gas mixtures as a function of drift field.

($40 \times 15 \times 40$ cm^3) and TPC2 ($45 \times 20 \times 40$ cm^3), are located in front of and behind D5, respectively. TPC1 and TPC2, although different in size, are of the same modular design. The field cages have the shape of a rectangular box designed to operate at atmospheric pressure. Voltage grading strips are mounted on the sides in order to obtain a uniform electric drifting field. The entrance and exit windows are 25 μm mylar foils. A gating grid is opened only for selected events and avoids back diffusion of positive ions into the drift volume.

An argon-methane (88%-12%) gas mixture is used near the saturation velocity with a 130 V/cm drift field. Other gas mixtures, cool and slow gases, for example argon-isobutane (75%-25%) at 800 V/cm drift field or neon-methane (90%-10%) at 300 V/cm, will be considered also, since they would lead to a smaller electron diffusion (Figure 6.7) both in the transverse and longitudinal directions, and thus to a smaller cluster size. Since the overall drift length in our TPC's is only of the order of 15 cm and because of the timing properties of the read-out electronics, we must use gas mixtures with i) relatively low drift velocity ($\approx$2 cm/μs) and ii) small longitudinal and transverse diffusion. New low mass gas mixtures such as He-C_2H_6, Ne-C_2H_6 and Ne-CO_2 are being tested with our prototype TPC.[2]

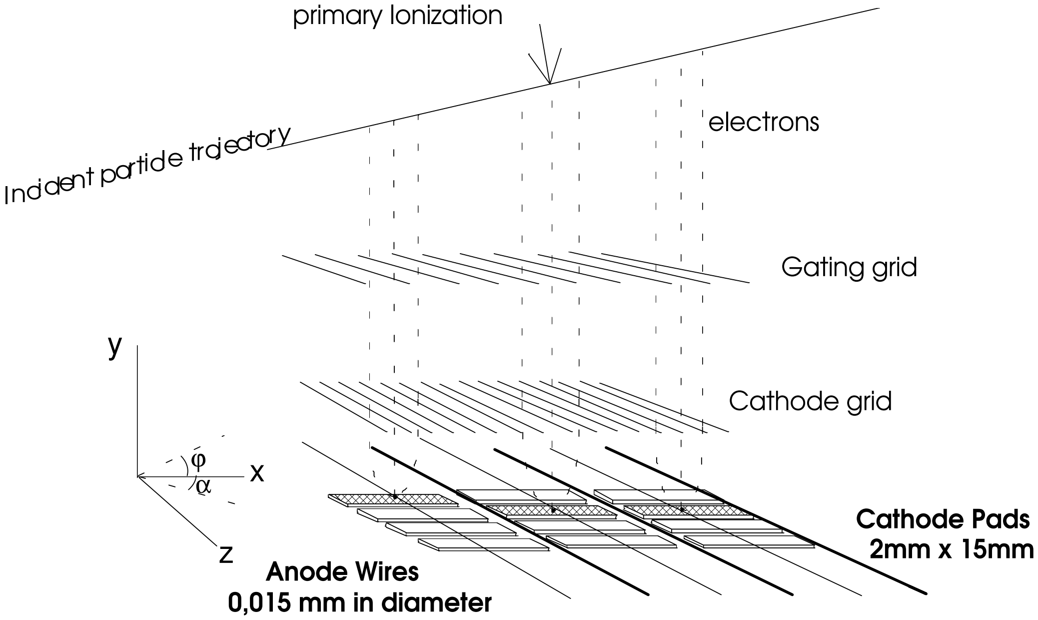

Figure 6.8: Schematic view of the pad-readout TPC.

Read out schemes

The primary ionization electrons drift toward the readout plane which contains thin gap (3 mm) proportional counters. Two usual readout schemes, either multiple anode wires or pad planes, are implemented in the prototype TPC we have built and are under test for spatial resolution capabilities. These read-out planes are of modular construction: each module consists of two read-out rows typically 38 cm long and 6 cm wide. Any number of these modules can then be assembled to build TPC's of desired depth to obtain the required momentum resolution and two-track separation. Such assemblies could be used not only for the two midrapidity TPC's but also for the Forward Arm Spectrometer tracking devices T1, T2 and possibly T3 .

Anode wire readout

The anode wire readout, previously used by another experiment (NA36)[1], consists of an anode plane divided into 10 identical rows located 2 mm above a solid copper cathode plane and 2 mm below a grid plane. Each row has 96 sense and field wires on a 2 mm pitch which are 20 μm and 50 μm in diameter, respectively. The gating grid, 8 mm higher, passes the drifting electrons for accepted events only and thus limits positive ion build-up in the drift volume.

Pad plane readout

In the high-field region close to the multiplying anode wire an avalanche takes place. The resulting electrons are quickly collected on the anode wire (~ 1 ns), whereas the more slowly moving positive ions induce image charges on the underlying pads (Figure 6.8). By recording the induced charge on the rows of rectangular pads at regular short time intervals by Flash Analog-to-Digital Converters (FADC) one achieves three-dimensional localization of the tracks. Typically, for each particle track, a cluster of about 3 to 5 pads in each pad row are involved in this process (Figure 6.9). For each track segment, the drift time from the primary ionization site to the anode wire yields the y coordinate (vertical), whereas the induced signals on the pad row yield the x (pad row number) and z (drift time) coordinates in the pad row plane (horizontal).

The pulse height distribution of the induced signal on each pad, z_i, of such a cluster depends on the distance of the pad from the centroid, z, of the cluster. The resulting pulse height distribution, the Pad Response Function (PRF), is approximated by the gaussian function P_i:

$$P_i = A \cdot e^{-\frac{(z-z_i)^2}{2\sigma_z^2}},$$

where z is the cluster centroid coordinate and z_i the location of the i-th pad of length l. The charge distribution width σ_z is a function of the drift length L_{drift} and the transverse diffusion constant D_{trans}, and depends on the angle α at which an incident particle crosses the pad row:

$$\sigma_z^2 = \sigma_{PRF}^2 + D_{trans}^2 \cdot L_{drift} + \frac{(\ell \cdot tan\alpha)^2}{12}.$$

σ_{PRF} is the intrinsic pad response width due to charges induced by a single anode wire on the underlying pads and depends mainly on the geometric configuration of the anode wire and pad planes. In our configuration with 2×15 mm^2 pads located 3 mm below the anode wire plane, this value is estimated to be $\sigma_{PRF} \approx 3.1$ mm.

A similar relation holds for the charge distribution in the y drift direction:

$$\sigma_y^2 = \sigma_o^2 + D_{long}^2 \cdot L_{drift} + \frac{(\ell \cdot tan\lambda)^2}{12},$$

where D_{long} is the diffusion constant in the longitudinal drift direction, λ is the angle of the particle trajectory to the $x - z$ plane (the dip angle) and σ_0 is the quadratic sum of a time slice of the FADC and the shaping time width (FWHM) of the preamplifiers:

$$\sigma_o^2 = \left(\frac{FWHM}{2.36}\right)^2 + \left(\frac{\Delta t}{\sqrt{12}}\right)^2.$$

The prototype is now undergoing a first series of tests with the following conditions:

- Argon-methane (90%-10%) gas mixture at 130 V/cm.
- 12.5 μm diameter anode wire.

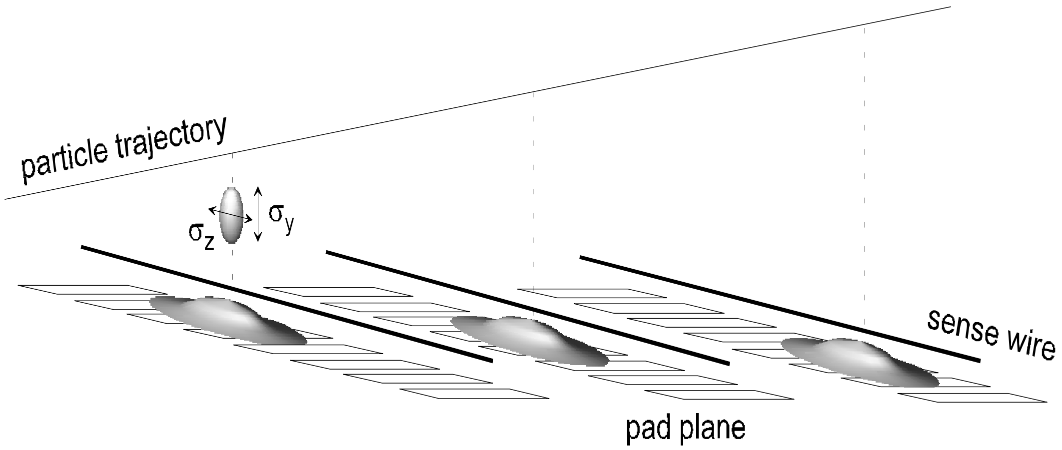

Figure 6.9: Typical geometry of the anode wires and pad rows with clusters.

- 3 mm cathode - anode wire gap, 3 mm anode wire - pad plane gap.
- 4 pad rows of 96 (2×15) mm^2 pads on a 4 mm pitch.

As an alternative to this rather conventional readout plane design, we are considering the use of a microstrip gas chamber (MSGC) analog design.[6] The multiplying anode wires are deposited atop a thin glass substrate, the pads being on the opposite surface of the substrate. Such an assembly could easily be reproduced as a large number of modules with minimum dispersion in geometric characteristics; furthermore, the smaller distance between anode and pad plane would improve the pad response function. A 50×50 mm^2 prototype has been build at GSI Darmstadt[4] following the original Oed[5] design with 8 μm wide anodes on a 1 mm pitch on a 300 μm glass substrate. A second prototype, different in the pad plane layout, is being designed at CRN Strasbourg where the MSGC technique has been used successfully[7]; nevertheless the achieved gas gain for stable operation has been limited as of this writing to a value of about 1000. Those prototypes will undergo extensive testing for pad response function and gain stability within the next two months. The size of the MSGC is as yet limited to 100×200 mm^2 by the available tools, and thus the readout plane would be constructed as an assembly of that size modules which does not carry further disadvantages.

6.3.2 Electronics

For the prototype tests we are using readout electronics which are similar to those used by the ALEPH and NA35 Collaborations (Figure 6.10), consisting of 16-channel preamplifier cards mounted directly to the TPC with their outputs led 4 by 4 via ~40 m

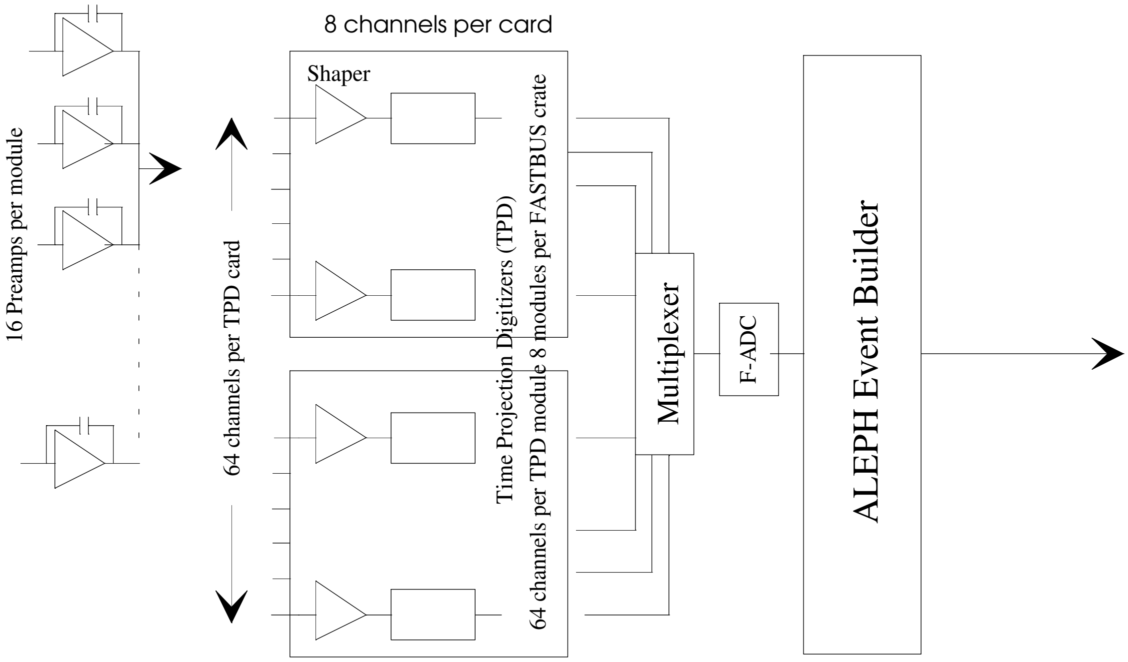

Figure 6.10: TPC readout electronics used by ALEPH and NA35.

long cables to Time Projection Digitizers (TPD) Fastbus modules. Each TPD module contains 64 shaping amplifiers and an FADC. A Fastbus crate contains 8 TPD's for a total of 512 channels and is read out by an ALEPH Event Builder (AEB). The FWHM of those shaping amplifiers is 180 ns and the clock frequency for sampling is 12.5 MHz, giving time slices of 80 ns width.

We are considering other highly integrated solutions for the final readout electronics to be used in the future: i) electronic systems designed at LBL for the NA49 and STAR Collaborations[3]; ii) new developments at the Laboratoire d'électronique et de Physique des systèmes Instrumentaux (LEPSI) at the University of Strasbourg.

The front end electronics (FEE) will be directly mounted on the TPC's read-out plane. Each $\approx 10\times 10$ cm^2 FEE card holds 32 channels providing: charge sensitive preamplifier, shaping amplifier, 265-samples analog storage (Switched Capacitor Array) analog-to-digital converter, zero suppression and multiplexed transmitter to the VME data processing.

6.3.3 TPC Characteristics

Position resolution

The ionization along a particle track yields an average number, n_o, of electron-ion pairs per centimeter of track length. Landau fluctuations affect the charge distribution centroid position in the particle track direction x. Since one assumes the x coordinate of the projected track to be at the center of a pad one has to account for that centroid shift in the position resolution in both the y and z coordinates. This is taken care of in the angle-dependent terms of the charge distribution relations by an empirical term, n_{eff}, related to the number of electron-ion pairs which effectively reach a pad along its length. To estimate the position resolution of our prototype TPC, we will use the value $n_{eff} = 15$ previously determined for minimum ionizing particles in similar designs. The expected position resolutions are then:

$$\partial_z^2 = \frac{\sigma_{PRF}^2 + D_{trans}^2 \cdot L_{drift}}{n_o \cdot \ell} + \frac{(\ell \cdot tan\alpha)^2}{12 \cdot n_{eff}}$$

$$\partial_y^2 = \frac{\sigma_o^2 + D_{long}^2 \cdot L_{drift}}{n_o \cdot \ell} + \frac{(\ell \cdot tan\lambda)^2}{12 \cdot n_{eff}}.$$

Assuming for minimum ionizing particles $n_o = 90$, $n_{eff} = 15$, and using the estimated values for our prototype from Table 6.8, one obtains:

$$\partial_z^2 = (0.266mm)^2 + (0.047mm)^2 \cdot L_{drift} + (1.12 \cdot tan\alpha)^2 = (335\mu m)^2$$

$$\partial_y^2 = (0.358mm)^2 + (0.0095mm)^2 \cdot L_{drift} + (1.12 \cdot tan\lambda)^2 = (360\mu m)^2.$$

The prominent terms in the position resolution are the diffusion constants which could be reduced by using other gas mixtures but which would in turn require a shorter integration time in the shaping amplifiers. This would affect the formation of the output signals and result in a decrease of their amplitude if the drift velocity is not significantly decreased. Since the pad-crossing and dip-angles are rather small in our design, increasing the pad length could improve the position resolution (increasing the pad length by factor of 2 could improve the position resolution by a factor of $\sqrt{2}$.)

Coordinate determination

For each accepted event, before performing the track-finding procedure one has to extract the coordinates x, y and z from the recorded signals. The coordinate x is the pad row number and y is determined by a weighted average of the pulse height P_{ij} :

$$y = \frac{\sum_{i,j} y_j P_{ij}}{\sum_{i,j} P_{ij}}$$

where P_{ij} is the pulse height of time slice j on pad number i. The coordinate along a pad row z is generally obtained from a weighted mean of the Pad Response Function P_i:

$$z = \frac{\sum z_i P_i}{\sum P_i}.$$

The procedure may be slightly different if only two or three pads are in a cluster.

If the cluster contains only two valid pad signals P_1 and P_2, their distribution is fitted using the function:

$$P_i = A \cdot e^{-\frac{(z-z_i)^2}{2\sigma_z^2}}$$

and then:

$$z = z_i + \frac{\Delta}{2} + \frac{\sigma_z^2}{\Delta} \cdot \ln \frac{(P_{i+1})}{(P_i)}.$$

For example, in a simplified way:

$$z = z_1 + \frac{\Delta}{2} + \frac{\sigma_z^2}{\Delta} \cdot \ln \frac{P_2}{P_1}$$

where z_1 is the position of the first pad in the cluster, Δ is the pad spacing (pad pitch) and σ_{PRF} is set to the expected value for the present design (Table 6.8.)

For a three pad cluster one can fit σ_{PRF} or σ_z as well by using a similar function or by using the following relations:

$$z = z_1 + \frac{\Delta}{2} + \frac{\sigma_{PRF}^2}{\Delta} \cdot \ln \frac{P_2}{P_1} = z = z_2 + \frac{\Delta}{2} + \frac{\sigma_z^2}{\Delta} \cdot \ln \frac{P_3}{P_2} = z = z_1 + \Delta + \frac{\Delta}{2} + \frac{\sigma_z^2}{\Delta} \cdot \ln \frac{P_3}{P_2}$$

$$\sigma_{PRF}^2 = \Delta^2 / \ln \frac{P_2^2}{P_1 P_3}.$$

With these conditions and the present prototype the relevant parameters are given in Table 6.8.

6.3.4 TPC Simulations

The rapidity and transverse momentum acceptance of the mid-rapidity spectrometer has been evaluated for Au + Au ($\sqrt{s}$ = 200 GeV/nucleon pair) events generated by VENUS through GEANT simulations. In order to simulate the processes in a TPC, each particle track was followed into the TPC and hits were generated for each track segment crossing the active volume above a pad row. A set of x, y, z coordinates was attributed to every

Parameter	Value
D_{trans}	550 μm/$\sqrt{\text{cm}}$
D_{long}	350 μm/$\sqrt{\text{cm}}$
σ_{PRF}	3.1 mm
σ_0	80 ns ; 5.2mm
v_{drift}	52 μm/ns
$\left(L_{drift}\right)_{max}$	20 cm
l	15 mm
α_{max}	5°
λ_{max}	15°

Table 6.8: TPC parameters for the present prototype.

hit. From hit coordinates y and z, a cluster was generated, taking into account the charge distribution deduced from energy loss calculations including Landau fluctuations and the parameterization outlined in the previous section, depending on drift length and trajectory angles. From those cluster parameters a two-dimensional gaussian shape charge distribution was calculated. The corresponding digitized values were attributed to each pad and time slice (bucket).

Such simulations are used to check the track recognition and reconstruction algorithms versus momentum resolution and will be used to test the two-track resolution capabilities of the spectrometer. This is of special interest if one wants to perform HBT analysis in order to obtain information on the space-time dimension of an emitting source. The momentum resolution and the two-track separation will set a lower limit for measurements of the Lorentz-invariant four-momentum difference $Q_{inv} = \sqrt{\sum_{x,y,z}(p_{xi} - p_{xj})^2 - (E_i - E_j)^2}$ of two identical particles.

Track finding and reconstruction

The tracking in the TPC's is performed, for present purposes, by utilizing a program adapted from an existing program designed for a silicon telescope (by A. and M.E. Michalon) used in the WA97 Experiment. This Track Pattern Recognition (TPR) program is comprised of three successive executive procedures :

- TPH, which builds the hits from the measured digits.
- TPA, which performs the optimized track recognition.
- TPO, which extracts the TPA-analysis results and stores them in ZEBRA data banks.

The TPH Procedure

This program selects the raw data monitored by the pad monitor program and extracted from the various cathode-pad planes of the TPC. For each plane the raw data are stored and converted into hits characterized by their DRS (Detector Reference System) coordinates.

The TPA Procedure
The Final Cluster-Distribution Elaboration

The program proceeds first to a "cleaning" to simplify the adjacent hit distribution (cluster) in the following manner :

- For a low number of adjacent hits (≤ 3) they are merged into a single hit located at the centroid of the initial distribution.
- For a medium number (≤ 6) they are merged into several clusters reflecting the sub-structure of the initial distribution.
- For a large number (> 6) they are rejected (often resulting from tracks perpendicular to the longitudinal axis of the TPC's, δ-rays, etc.).

This defines the set of hits as illustrated in top frames of Figure 6.11.

Iterations are then performed on three subprocesses:

1. tolerance definition
2. track following
3. track road.

Pre-Processing of Hits in Following Tracks

This procedure is applied simultaneously to the $x - y$ and $x - z$ planes. Scanning starts from the back of the TPC (the last plane of hits) where the hit density is lowest. For each hit one defines a window F_0 by a cone with the apex located at the hit and whose opening angle (an adjustable parameter) is such that it covers the whole (or a large fraction) of the front face of the TPC. All the hits contained in this plane are analyzed separately and simultaneously in this way. Then, one scrutinizes the hits in the precedent (next to last) plane which are contained in the defined window. By analyzing the statistical distribution of these hit locations, one defines the most probable location

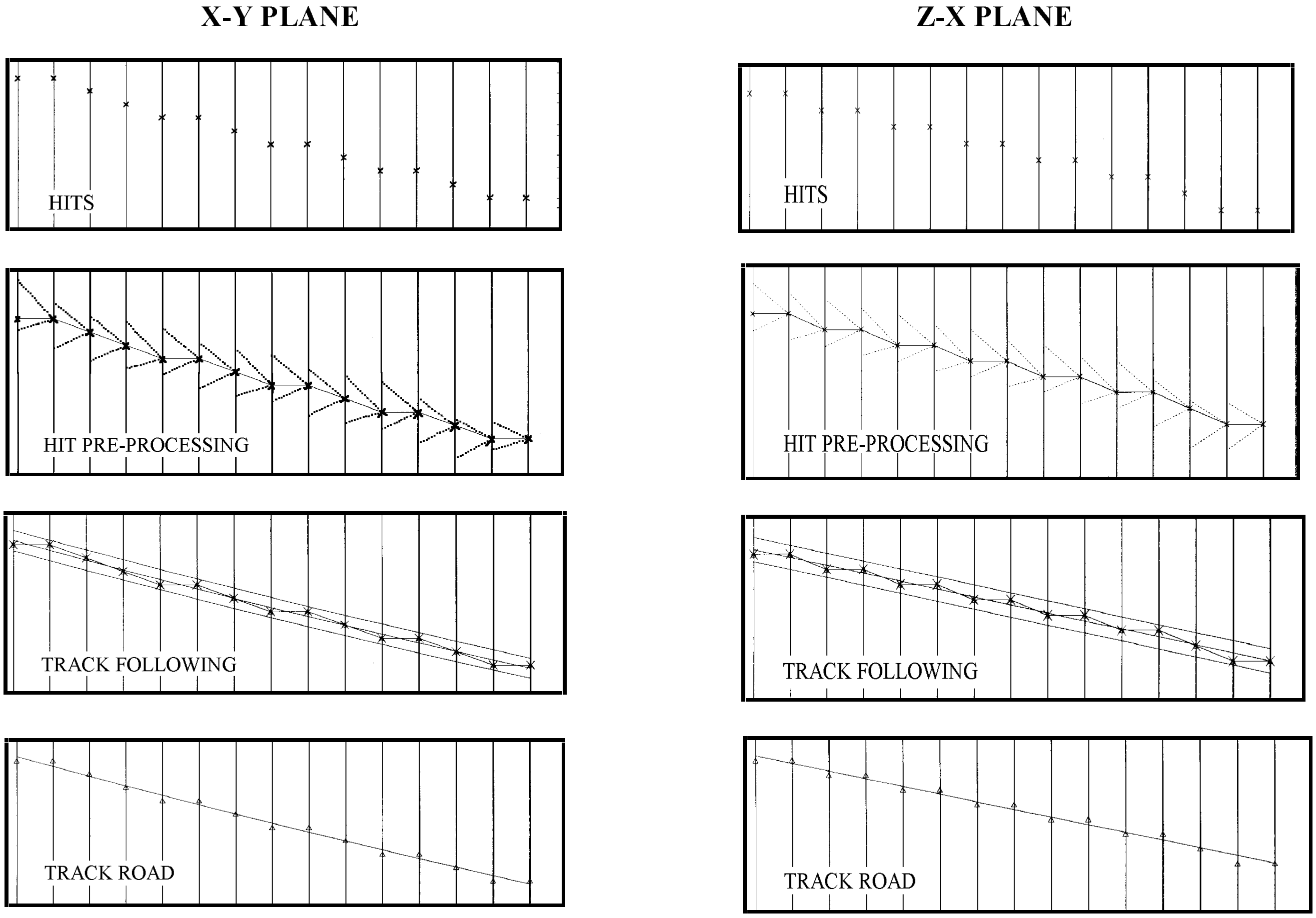

Figure 6.11: Illustration of the steps used in track finding and reconstruction.

(the centroid of the distribution) of the hit associated with that considered, as well as the opening of the next window F_1 (the width of the distribution). This defines a segment, a possible track-element, extending from the initial hit location to the new one found. The procedure is then iterated by considering next the plane immediately before, and so on. For each new plane the opening of the window is adjusted (i.e., reduced) accordingly. This procedure is illustrated in the second from top frames of Figure 6.11.

When one single initial hit is followed by a gap (no hit in the next plane) the process is aborted for this specific investigation. This, of course, is not relevant when a gap (or more) occurs after several hits, i.e., shorter tracks.

Following Tracks and Determining the Track Road

The aim is to determine the *most probable complete track* from the collection of segments obtained. Thus, the segments are associated to generate possible tracks and then they are sorted out. When several tracks share common hits these latter are associated with the longest track. Tracks with only few spare hits are eliminated. When hits are missing (no hits are close to the impact of the possible track) in a particular plane then ghost hits are created. In this way possible tracks are constituted with different level of confidence.

By linear fitting to the possible tracks and by adding a given variance (a parameter) to this fit, one determines a possible road as shown in the second from bottom frames of Figure 6.11. The number of hits included in the calculated road determines the quality of the result and whether a new iteration should be considered. Used hits in the track road determination are flagged and their number should be equal to the number of analyzed planes. Concretely the width of the road is increased until the number of hits remains constant and close to the number of planes. The final track, together with the initial hits, are shown in the bottom frame of Figure 6.11. Unused hits not belonging to the road under construction are restituted to be included in further analyses of other tracks.

6.3.5 Present Status

At this point the prototype TPC, including the two mentioned readout schemes, has been built at the Centre de Recherches Nucléaires, Strasbourg, France. Preliminary tests of the field cage and the readout systems have been satisfactorily achieved using radioactive sources (electrons and X rays).

For further testing, the prototype has now been moved to the Gesellschaft fur Schwerionen Forschung (G.S.I.) at Darmstadt, Germany. At present we have 512 channels of electronics (preamplifiers, TPD's) connected to a computer via an ALEPH Event Builder. Extensive tests using radioactive sources and laser beams have been undertaken in order to measure the basic performance in space resolution and two-track separation of the prototypes.

References

1. C. Garabalos, Nucl. Instrum. and Meth. **A283**, 553 (1989).

2. J. Va'vra, P. Coyle, J. Kadyk and J. Wise, Nucl. Instrum. and Meth. **A324**, 113 (1993).

3. A. Mock, Diplomarbeit, Technische Universitat Munchen.

4. H. Sahn, GSI, Darmstadt, private communication.

5. A. Oed, Nucl. Instrum. and Meth. **A263**, 351 (1988).

6. R&D-32 Status Report, CERN/DRDC 94-10.

7. A. Pallares *et al.*, Internal Report, CRN Strasbourg (1994).